Enhancing efficiency and scope of first-principles quasiharmonic approximation methods through the calculation of third-order elastic constants

Adewumi Bakare and Angelo Bongiorno
Department of Chemistry, College of Staten Island, Staten Island, New York 10314, USA
and The Graduate Center of the City University of New York, New York, New York 10016, USA

(Received 27 June 2021; revised 18 February 2022; accepted 28 March 2022; published 15 April 2022)

A novel computational strategy is presented to calculate from *first principles* the coefficient of thermal expansion and the elastic constants of a material over meaningful intervals of temperature and pressure. This strategy combines a novel implementation of the quasiharmonic approximation to calculate the isothermal-isochoric linear and nonlinear elastic constants of a material, with elementary equations of nonlinear continuum mechanics. Our implementation of the quasiharmonic approximation relies on finite deformations, the use of nonprimitive supercells to describe a material, a recently proposed technique to calculate generalized mode Grüneisen parameters, and the numerical differentiation of the stress tensor to calculate both second- and third-order elastic constants. The combination of this method with nonlinear continuum mechanics is shown to yield accurate predictions of lattice parameters and linear elastic constants of a material over finite intervals of temperature and pressure, at the cost of calculating isothermal second- and third-order elastic constants for a single reference state. Here, the validity and limits of our novel methods are assessed by carrying out calculations of MgO based on classical interatomic potentials. To demonstrate potential, our methods are then used in conjunction with a density functional theory approach to calculate thermal expansion and elastic properties of silicon, lithium hydrate, and graphite.

DOI: 10.1103/PhysRevMaterials.6.043803

I. INTRODUCTION

Thermal expansion and elasticity are materials properties of both fundamental and technological importance [1–4]. Thermal expansion is a phenomenon arising from anharmonic behaviors of a solid material, and understanding and predicting thermal expansion properties are important, for example, to design reliable multicomponent devices operating at variable temperature [3,4]. Elastic constants are materials parameters of broad relevance. In geophysics, for example, second-order elastic constants (SOECs) are used to interpret seismic data [1,5–7], whereas in fields such as mechanical engineering and solid state physics, SOECs and third-order elastic constants (TOECs) are used to estimate the yield strength of random solid solution alloys [8,9], to calculate the ideal strength and predict the mechanical failure of metal alloys [10–16], and to characterize solid-solid phase transitions [17–20]. Although well-established experimental techniques are available to measure thermoelastic parameters [3,21,22], experimental data of thermal expansion coefficients, and SOECs and TOECs are available only for a subset of all known solid compounds, and often only at selected values or narrow intervals of temperature and pressure [21,23–28]. Computational methods for the routine calculation of thermoelastic parameters are needed not only to compensate the lack of experimental data [29], but also to enable thermoelastic studies of materials at conditions difficult to attain experimentally [30,31], as well as to facilitate the high-throughput screening [29,32] of useful mechanical parameters at relevant environmental conditions, such as the ideal strength of metal alloys for structural applications [12–16]. In this work, we present a novel computational strategy to calculate from first principles the coefficient of thermal expansion and the elastic constants of a material over meaningful intervals of temperature and pressure. This strategy is based the use of a novel implementation of the quasiharmonic approximation to calculate the isothermal-isochoric linear and nonlinear elastic constants of a material, followed by an extrapolation procedure relying on nonlinear continuum mechanics.

Quasiharmonic approximation (QHA) methods are suited to calculate thermodynamic and thermoelastic parameters of materials at temperatures and pressures at which dynamical anharmonic effects are small and can be disregarded [33–39]. In general, QHA methods give accurate results at low up to moderate temperatures [32,34–42]. At high temperatures, dynamical anharmonic effects play an important role, and results obtained from QHA can be corrected through the use of empirical models or thanks to the aid of molecular dynamics techniques [43–45]. The calculation of thermal expansion coefficients and SOECs through the use of a conventional QHA method involves the following tasks [32,34–42]. First, carrying out phonon calculations to calculate the harmonic Helmholtz free energy function for a list of deformed configurations of a solid material in a neighborhood of a reference state. Second, using an equation of state (e.g. Murnaghan's [46] or Vinet's [47]) or a polynomial function to interpolate the free energy values of the various configurations and calculate lattice parameter and bulk modulus at selected values of

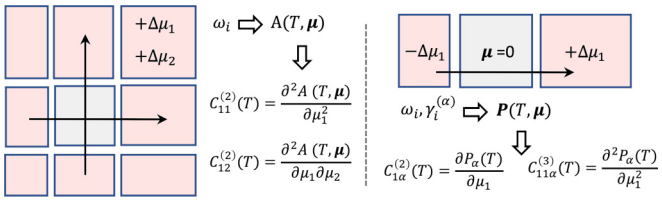

FIG. 1. Schematic illustration of the key ingredients of conventional (left) and present (right) implementations of QHA to calculate thermoelastic parameters of a material. Both implementations rely on generating a set of deformed configurations (light red) of a reference state (light gray); μ is the Lagrangian strain, and for convenience, tensor components are indexed using the Voigt notation. In the conventional approach, SOECs are obtained via second-order differentiation of the Helmholtz free energy (A), whereas the present approach relies on the calculation of the generalized mode Grüneisen parameters ($\gamma_i^{(\alpha)}$) to obtain SOECs and TOECs via first- and second-order differentiation of the second Piola-Kirchhoff stress tensor (P), respectively.

temperature and pressure. Third, for given values of temperature and pressure, and hence lattice parameters, calculation of phonon frequencies for a grid of strained configurations, and calculation of SOECs via second-order differentiation of the Helmholtz free energy with respect to strain (Fig. 1). This implementation of QHA is straightforward [32,34–42]. However, in general it requires to consider numerous configurations of a material, and therefore it suffers from an intricate workflow, which is typically manageable only in the case of materials with the cubic symmetry. For example, in the case of a hexagonal material, existing QHA methods employ a grid of at least 25 deformed configurations of a reference state to calculate the two lattice parameters as a function of temperature [48], and an additional ∼15 deformed configurations to calculate the five independent SOECs at any selected values of the temperature and pressure [41,48]. It is not surprising that over the past years, alternative [49] and approximate [41] QHA-based approaches have been put forward to investigate the thermoelastic properties of the vast class of materials not belonging to the cubic crystal system.

In this work, we present an implementation of QHA to calculate isothermal-isochoric SOECs and TOECs of a solid material that involves a reduced workload and requires a minimal number of deformed configurations of a reference state. In detail, our QHA approach requires four deformed configurations, including the reference state, to calculate the independent isothermal SOECs of a cubic material at constant volume, and an additional 4 configurations to also calculate the independent TOECs. To calculate the 5+10 and 9+20 independent SOECs and TOECs of hexagonal and orthorhombic systems, these two numbers become 6 and 6, and 10 and 8, respectively. Furthermore, in this work we show that knowledge of the isothermal-isochoric SOECs and TOECs of a material in a reference state allows to estimate, within the framework of nonlinear continuum mechanics, lattice parameters, and SOECs in a meaningful neighborhood of the reference state, or equivalently, within intervals of temperature and pressure inducing deformations of the reference state of a few percents in strain. Overall, here we show that combination of our new QHA method to calculate SOECs and TOECs with elementary equations of nonlinear continuum mechanics consists of a computationally efficient strategy to investigate thermoelastic properties of materials from first principles.

This manuscript is organized as follows. In Sec. II, we introduce basic concepts and definitions of finite strain theory and nonlinear elasticity. In Sec. III, we present our implementation of QHA to calculate isothermal-isochoric SOECs and TOECs. In this section, we also provide details about both the approach used to calculate generalized mode Grüneisen parameters and the finite differentiation techniques used to calculate linear and nonlinear elastic constants. In Sec. IV, we present our new computational strategy combining the present QHA method with nonlinear continuum mechanics to calculate thermoelastic parameters of a material in a neighborhood of a reference state. In Sec. V, we demonstrate validity and assess limits of our methods by carrying out calculations of MgO based on classical interatomic potentials [50]. In Sec. VI, we discuss technical aspects and results obtained by applying our methods in combination with a density functional theory approach to calculate selected thermoelastic properties of silicon, lithium hydride, and graphite. A summary of our work and a discussion of the potential applications of our methods are reported in Sec. VII.

II. NOTIONS OF NONLINEAR CONTINUUM MECHANICS

Here we consider solid materials described at the atomistic level by using either classical interatomic potentials [50] or a periodic density functional theory (DFT) approach [51,52]. With $\boldsymbol{V}$ we indicate the 3×3 matrix whose columns, $\vec{a}_1$, $\vec{a}_2$, and $\vec{a}_3$, are the vectors defining the geometry of the supercell used to describe the material in a reference state. Each point of the undeformed material can be referenced by using a coordinate system X_i $(i = x, y, z)$. With $\boldsymbol{V'}$ we indicate the 3×3 matrix defining the geometry of the supercell describing the material that has undergone a homogeneous deformation. Points of the deformed material are referenced by using the coordinate system x_i. Each point of the undeformed material is mapped onto a point of the deformed material, and the gradient of the mapping function $\vec{x}(\vec{X})$ defines the deformation gradient $\boldsymbol{F}$, a second-order tensor whose components are defined as follows:

$$F_{ij} = \frac{\partial x_i}{\partial X_j} = V'_{ik} V^{-1}_{kj}, \tag{1}$$

where the first equality gives the general definition of $F_{ij}(\vec{X})$ in terms of deformed (x_i) and undeformed (X_j) coordinates, whereas the second equality shows how $\boldsymbol{F}$ relates to $\boldsymbol{V}$ and $\boldsymbol{V'}$ in case of a homogeneous deformation.

In nonlinear continuum mechanics [2], deformations are commonly described by using the Green-Lagrangian strain tensor, $\boldsymbol{\mu}$, which is related to $\boldsymbol{F}$ as follows:

$$\boldsymbol{\mu} = \tfrac{1}{2}(\boldsymbol{F}\boldsymbol{F}^T - \mathbf{I}), \tag{2}$$

where $\mathbf{I}$ is the identity matrix. To the third order in the Lagrangian strain, the Helmholtz free energy of a material

$A(T, \boldsymbol{\mu})$ can be written as follows:

$$\frac{A(T,\boldsymbol{\mu})}{V} = C^{(1)}_{ij}\mu_{ij} + \frac{1}{2}C^{(2)}_{ijkl}\mu_{ij}\mu_{kl} + \frac{1}{6}C^{(3)}_{ijklmn}\mu_{ij}\mu_{kl}\mu_{mn}, \quad (3)$$

where V is the volume of the reference state, tensor indexes refer to cartesian axes, $C^{(1)}_{ij}$ is the internal stress tensor of the material in the reference state, and $C^{(2)}_{ijkl}$ and $C^{(3)}_{ijklmn}$ are the isothermal SOECs and TOECs of the material at constant volume in the reference state. $C^{(1)}_{ij}$, SOECs, and TOECs in Eq. (3) are all functions of the temperature, with SOECs and TOECs defined as

$$C^{(2)}_{ijkl} = \frac{1}{V}\left.\frac{\partial^2 A(T,\boldsymbol{\mu})}{\partial\mu_{ij}\partial\mu_{kl}}\right|_{\boldsymbol{\mu}=\mathbf{0}},$$
$$C^{(3)}_{ijklmn} = \frac{1}{V}\left.\frac{\partial^3 A(T,\boldsymbol{\mu})}{\partial\mu_{ij}\partial\mu_{kl}\partial\mu_{mn}}\right|_{\boldsymbol{\mu}=\mathbf{0}}. \quad (4)$$

We underline that the definitions in Eq. (4) are valid also when the reference state is subjected to an external stress, and hence $C^{(1)}_{ij}$ is not null. In this latter case, however, the mathematical definitions in Eq. (4) need to be reconciled with physical parameters measured experimentally, as for example in case of the relationship between (Cauchy) stress and strain:

$$\sigma_{ij} = B^{(2)}_{ijkl}\mu_{kl}, \quad (5)$$

for which it can be shown [53] that the experimental second-order elastic coefficients $B^{(2)}_{ijkl}$ are related to the SOECs defined in Eq. (4) as follows:

$$B^{(2)}_{ijkl} = C^{(2)}_{ijkl} + \tfrac{1}{2}\big(C^{(1)}_{il}\delta_{jk} + C^{(1)}_{jl}\delta_{ik} + C^{(1)}_{ik}\delta_{jl} + C^{(1)}_{jk}\delta_{il} - 2C^{(1)}_{ij}\delta_{kl}\big). \quad (6)$$

The coefficients $B^{(2)}_{ijkl}$ and Eq. (6) are important when, for example, SOECs defined as in Eq. (4) are used to calculate the elastic moduli of a material in a stressed reference state.

The definitions in Eq. (4) can be rewritten in terms of the second Piola-Kirchhoff (PK2) stress tensor, which is defined as follows:

$$P_{ij}(\boldsymbol{\mu}) = \frac{1}{V}\left.\frac{\partial A(T,\boldsymbol{\mu})}{\partial\mu_{ij}}\right|_{\boldsymbol{\mu}=\mathbf{0}}. \quad (7)$$

In particular, from Eqs. (3) and (4), we find

$$P_{ij}(\boldsymbol{\mu}) = C^{(1)}_{ij} + C^{(2)}_{ijkl}\mu_{kl} + \tfrac{1}{2}C^{(3)}_{ijklmn}\mu_{kl}\mu_{mn}, \quad (8)$$

with

$$C^{(2)}_{ijkl} = \left.\frac{\partial P_{ij}(\boldsymbol{\mu})}{\partial\mu_{kl}}\right|_{\boldsymbol{\mu}=\mathbf{0}},$$
$$C^{(3)}_{ijklmn} = \left.\frac{\partial^2 P_{ij}(\boldsymbol{\mu})}{\partial\mu_{kl}\partial\mu_{mn}}\right|_{\boldsymbol{\mu}=\mathbf{0}}, \quad (9)$$

where

$$C^{(1)}_{ij} = P_{ij}(\boldsymbol{\mu}=\mathbf{0}) = \sigma_{ij}, \quad (10)$$

i.e., Cauchy stress and PK2 stress are equivalent in the reference state. In general, the relationship between Cauchy stress and PK2 stress of a material in a deformed state is

$$\mathbf{P} = \det|\mathbf{F}|\mathbf{F}^{-1}\boldsymbol{\sigma}\mathbf{F}^{-T}, \quad (11)$$

where $\boldsymbol{F}$ is the deformation gradient mapping the reference state $\boldsymbol{V}$ onto the deformed state $\boldsymbol{V}'$, and $\boldsymbol{\sigma}$ and $\boldsymbol{P}$ are Cauchy and PK2 stress tensors of the material in the deformed state $\boldsymbol{V}'$.

For convenience, in the following sections, we will use the Voigt notation to refer to tensor components. In detail, $P_{ij} \leftrightarrow P_\alpha$, $C^{(2)}_{ijkm} \leftrightarrow C^{(2)}_{\alpha\beta}$ and $C^{(3)}_{ijklmn} \leftrightarrow C^{(3)}_{\alpha\beta\gamma}$, with Voigt indexes α, β, and γ assuming values between 1 and 6, and related to pairs of Cartesian indexes as follows: $xx \to 1$, $yy \to 2$, $zz \to 3$, $yz \to 4$, $xz \to 5$, and $xy \to 6$.

III. QHA METHOD TO CALCULATE SOECS AND TOECS

Within QHA, thermoelastic parameters such as the coefficient of thermal expansion and the isothermal SOECs are typically obtained by calculating the harmonic Helmholtz free energy $A(T, V)$ for a list of deformed configurations of a reference state for a solid material [32,34–42]. For each configuration, the Helmholtz free energy is calculated as follows:

$$A(T,V) = E_0(V) + \frac{1}{N_{\boldsymbol{q}}}\sum_{\boldsymbol{q},\kappa}\frac{\hbar\omega_{\boldsymbol{q},\kappa}}{2} + \frac{k_BT}{N_{\boldsymbol{q}}}\sum_{\boldsymbol{q},\kappa}\ln\left[1-\exp\left(-\frac{\hbar\omega_{\boldsymbol{q},\kappa}}{k_BT}\right)\right], \quad (12)$$

where E_0 is the static energy of the material, $\omega_{\boldsymbol{q},\kappa}$ are the harmonic frequencies, $N_{\boldsymbol{q}}$ is the number of $\boldsymbol{q}$ points in the Brillouin zone, and κ is the branch index. Here we present an implementation of QHA that relies on the Cauchy stress tensor, rather than $A(T, V)$, to calculate the thermoelastic parameters. In particular, given a reference or a deformed configuration of a material, the components σ_α of the Cauchy stress tensor can be calculated within QHA as follows:

$$\sigma_\alpha(T,V) = \sigma^S_\alpha(V) + \frac{1}{N_{\boldsymbol{q}}V}\sum_{\boldsymbol{q},\kappa}\gamma^{(\alpha)}_{\boldsymbol{q},\kappa}\frac{\hbar\omega_{\boldsymbol{q},\kappa}}{2} + \frac{1}{N_{\boldsymbol{q}}V}\sum_{\boldsymbol{q},\kappa}\gamma^{(\alpha)}_{\boldsymbol{q},\kappa}\frac{\hbar\omega_{\boldsymbol{q},\kappa}}{\exp\left(\frac{\hbar\omega_{\boldsymbol{q},\kappa}}{k_BT}\right)-1}, \quad (13)$$

where $\gamma^{(\alpha)}_{\boldsymbol{q},\kappa}$ are components of the generalized mode Grüneisen parameters tensor [54] associated with the frequency $\omega_{\boldsymbol{q},\kappa}$. Here we employ a novel approach to calculate these parameters [54].

A. Generalized mode Grüneisen parameters

The conventional technique used to calculate mode Grüneisen parameters is based on the following equations:

$$\gamma^{(\alpha)}_{\boldsymbol{q},\kappa} = -\frac{1}{\omega_{\boldsymbol{q},\kappa}}\frac{\partial\omega_{\boldsymbol{q},\kappa}}{\partial\mu_\alpha} = \frac{1}{\omega^2_{\boldsymbol{q},\kappa}}\vec{e}^{\,*}_{\boldsymbol{q},\kappa}\frac{\partial\boldsymbol{D}(\boldsymbol{q})}{\partial\mu_\alpha}\vec{e}_{\boldsymbol{q},\kappa}, \quad (14)$$

where $\boldsymbol{D}(\boldsymbol{q})$ is the dynamical matrix at $\boldsymbol{q}$ and $\vec{e}_{\boldsymbol{q},\kappa}$ is the eigenmode associated with the frequency $\omega_{\boldsymbol{q},\kappa}$. Here, instead of Eq. (14), we use a novel method to calculate these parameters [54]. This method can be used to calculate mode parameters associated only with frequencies at Γ. In particular, it has been

recently shown [54] that, given a Γ-point normal mode with frequency ω_κ, the corresponding generalized mode Grüneisen parameter satisfies the following relations:

$$\gamma_\kappa^{(\alpha)} = \frac{V}{2\omega_\kappa^2}\frac{\partial^2\left[\sigma_\alpha - \sigma_\alpha^H\right]}{\partial q_\kappa^2} = \frac{V}{2\omega_\kappa^2}\frac{\partial^2\sigma_\alpha^A}{\partial q_\kappa^2}, \tag{15}$$

where q_κ is the normal mode coordinate associated with ω_κ, σ_α is the static Cauchy stress tensor, σ_α^H is the harmonic stress tensor, which can be expressed in terms of the real-space force constants matrix and ionic displacements [54], and σ_α^A is simply equal to $\sigma_\alpha - \sigma_\alpha^H$. In practice, the calculation of the tensors, $\boldsymbol{\gamma}_\kappa$, involves the following operations. First, an ionic relaxation calculation to release any internal stress (resulting, for example, from a homogeneous deformation), followed by the calculation of the normal mode frequencies and coordinates. Second, for each normal mode κ, two total energy calculations with ions fixed in a configuration accommodating displacements along the normal mode, with amplitudes $\pm q_\kappa$. Finally, the components of the mode-parameters tensor are calculated by using the following second-order central finite difference formula:

$$\gamma_\kappa^{(\alpha)} \approxeq V\frac{\sigma_\alpha^A[\zeta_\kappa] + \sigma_\alpha^A[-\zeta_\kappa] - 2\sigma_\alpha^A[0]}{\zeta_\kappa^2}, \tag{16}$$

where $\zeta_\kappa = \sqrt{2}q_\kappa\omega_\kappa$ and q_κ is the normal mode coordinate with a value such to obtain an increase of the potential energy with respect to equilibrium of a few tenth of an eV [54].

It is to be noted that, in contrast to existing techniques based on the use of Eq. (14), the method based on Eqs. (15) and (16) yields all the components of the generalized mode Grüneisen parameter tensors, and hence of the thermal stress tensor [Eq. (13)], by carrying out calculations at only the volume of interest. At the same time, however, this method yields only mode Grüneisen parameters associated with frequencies at Γ. Therefore, to obtain converged values of the thermal stress tensor in Eq. (13), the QHA method here presented [which relies on Eqs. (15) and (16) to calculate γ_κ] necessitates the use of nonprimitive supercells containing a sufficiently large number, 3N-3, of normal modes of vibration at Γ, where N is the number of atoms in the supercell.

B. Finite deformation method

To calculate SOECs and TOECs of a material at constant temperature and volume, we use the finite deformation approach. In particular, to calculate SOECs we use the following first-order central finite difference formula:

$$C_{\alpha\beta}^{(2)} = \frac{\partial P_\alpha}{\partial\mu_\beta} \approxeq \frac{P_\alpha^{(+\Delta\mu_\beta)} - P_\alpha^{(-\Delta\mu_\beta)}}{2\Delta\mu_\beta}, \tag{17}$$

where $P_\alpha^{(\pm\Delta\mu_\beta)}$ is the PK2 stress tensor arising in a deformed supercell accommodating the finite strains $\pm\Delta\mu_\beta$. To calculate TOECs, we have the following two cases. One, TOECs with either two or three equal (Voigt) indexes are calculated by using the following second-order central finite difference formula:

$$C_{\alpha\beta\beta}^{(3)} = \frac{\partial^2 P_\alpha}{\partial{\mu_\beta}^2} \approxeq \frac{P_\alpha^{(+\Delta\mu_\beta)} + P_\alpha^{(-\Delta\mu_\beta)} - 2P_\alpha^{(\mathbf{0})}}{{\Delta\mu_\beta}^2}, \tag{18}$$

where $P_\alpha^{(\mathbf{0})}$ is the PK2 (equal to the Cauchy) stress tensor of the material in the reference state. Two, TOECs with three unequal (Voigt) indexes are calculated by using the following finite difference formula:

$$C_{\alpha\beta\gamma}^{(3)} \approxeq \left(P_\alpha^{(+\Delta\mu_\beta,+\Delta\mu_\gamma)} - P_\alpha^{(-\Delta\mu_\beta,+\Delta\mu_\gamma)} - P_\alpha^{(+\Delta\mu_\beta,-\Delta\mu_\gamma)} + P_\alpha^{(-\Delta\mu_\beta,-\Delta\mu_\gamma)}\right)/4\Delta\mu_\beta\Delta\mu_\gamma. \tag{19}$$

In this latter case, the PK2 stress tensor is calculated for deformed configurations of a reference state accommodating two different finite deformations, $\pm\Delta\mu_\beta$ and $\pm\Delta\mu_\gamma$.

Equations (17)–(19) can be used to calculate the isochoric SOECs and TOECs of a material in a stressed or unstressed reference state, at both zero or finite temperature. In practice, the calculation of the elastic constants involves the following elementary steps. One, selection of a reference state and a nonprimitive supercell with geometry and volume specifed by $\boldsymbol{V}$. Two, generation of the list of finite deformations required to calculate the independent SOECs and TOECs via Eqs. (17)–(19). Three, for each deformed supercell $\boldsymbol{V}'$, calculation of the generalized mode Grüneisen parameters tensors and Cauchy thermal stress tensor in Eq. (13). Lastly, Eq. (11) is used to calculate the PK2 stress tensors resulting from the finite deformations, and Eqs. (17)-(19) are used to calculate the linear and nonlinear elastic constants. In a schematic form, the aforementioned operations can be outlined as follows:

$$\boldsymbol{V} \xrightarrow{\boldsymbol{\mu}} \boldsymbol{F}, \boldsymbol{V}' \xrightarrow{(\boldsymbol{\sigma}^S, \omega_\kappa, \boldsymbol{\gamma}_\kappa)} \boldsymbol{\sigma}(T, \boldsymbol{\mu}) \xrightarrow{\boldsymbol{F}} \boldsymbol{P}(T, \boldsymbol{\mu}), \tag{20}$$

where the text above arrows specifies the quantities needed to accomplish each step, that is to derive the quantities on the right side from the quantities on the left.

To generate a deformed configuration of a reference state $\boldsymbol{V}$, we carry out the following elementary operations. One, we select a strain (Voigt) vector and construct the strain tensor $\boldsymbol{\mu}$ as follows:

$$(\xi_1 \quad \xi_2 \quad \xi_3 \quad \xi_4 \quad \xi_5 \quad \xi_6) \Rightarrow \boldsymbol{\mu} = \begin{pmatrix} \xi_1 & \xi_6/2 & \xi_5/2 \\ \xi_6/2 & \xi_2 & \xi_4/2 \\ \xi_5/2 & \xi_4/2 & \xi_3 \end{pmatrix}. \tag{21}$$

Two, we determine the deformation gradient $\boldsymbol{D}$ associated to $\boldsymbol{\mu}$ from Eq. (2) by carrying out a Cholesky decomposition of the following 3 × 3 matrix:

$$2\boldsymbol{\mu} + \mathbf{I} = \boldsymbol{D}\boldsymbol{D}^T. \tag{22}$$

Three, we carry out the single value factorization of $\boldsymbol{D}$, thus obtaining $\boldsymbol{D} = \boldsymbol{W}\boldsymbol{S}\boldsymbol{V}^T$, where $\boldsymbol{W}$ and $\boldsymbol{V}$ are unitary matrices, and $\boldsymbol{S}$ is the diagonal matrix of singular values. Four, we define the rotation-free deformation gradient (or right stretch tensor) as $\boldsymbol{F} = \boldsymbol{V}\boldsymbol{S}\boldsymbol{V}^T$ (whereas the rotation tensor is $\boldsymbol{R} = \boldsymbol{W}\boldsymbol{V}^T$). Lastly, the 3 × 3 matrix $\boldsymbol{V}'$ defining the geometry of the supercell for the material in the deformed state is obtained from Eq. (1) as follows: $\boldsymbol{V}' = \boldsymbol{F}\boldsymbol{V}$.

In diagram 20, $\boldsymbol{\mu}$ is either a single normal or pure shear strain or, in case of selected TOECs, the combination of two such elementary strains [55]. In particular, to calculate the 3+6 independent SOECs and TOECs of a material with the

cubic symmetry, we use the following list of finite deformations, which we express in terms of Lagrangian strain (Voigt) vectors:

$$\begin{aligned}
&1 \rightarrow (0 \quad 0 \quad 0 \quad 0 \quad 0 \quad 0);\\
&2 \rightarrow (\pm\xi \quad 0 \quad 0 \quad 0 \quad 0 \quad 0);\\
&3 \rightarrow (0 \quad 0 \quad 0 \quad +\xi \quad 0 \quad 0);\\
&4 \rightarrow (\pm\xi \quad \pm\xi \quad 0 \quad 0 \quad 0 \quad 0), (+\xi \quad -\xi \quad 0 \quad 0 \quad 0 \quad 0);\\
&5 \rightarrow (0 \quad 0 \quad 0 \quad +\xi \quad +\xi \quad 0);
\end{aligned} \tag{23}$$

where ξ is the strain parameter, typically taking values between 0.005 and 0.0150. In the list above, the zero strain vector labeled '1' corresponds to the reference state, the two vectors labeled "2" allow to calculate $C_{11}^{(2)}$, $C_{12}^{(2)}$, $C_{111}^{(3)}$, and $C_{112}^{(3)}$, the deformation labeled "3" allows to calculate $C_{44}^{(2)}$, $C_{144}^{(3)}$, and $C_{244}^{(3)} = C_{155}^{(3)}$, the three vectors labeled "4" allow to calculate $C_{123}^{(3)}$, and the vector "5" yields $C_{456}^{(3)}$. Thus, our QHA method allows to calculate the 3+6 independent SOECs and TOECs of a cubic material by carrying out calculations (of static energies and stress tensors, phonon frequencies, and generalized mode Grüneisen parameters tensors) for a total list of 8 configurations of the material (including the reference state). It is to be noted that the list in 23 excludes configurations that, due to cubic symmetry, yield redundant results. For example, the two deformations

$$(+\xi \quad -\xi \quad 0 \quad 0 \quad 0 \quad 0), (-\xi \quad +\xi \quad 0 \quad 0 \quad 0 \quad 0) \tag{24}$$

give the same value of P_3 in case of a cubic material, and therefore only one of them is retained in the list above to calculate $C_{123}^{(3)}$ via Eq. (19). For the same reason, to calculate $C_{456}^{(3)}$, we only need one of the following four deformations:

$$(0 \quad 0 \quad 0 \quad \pm\xi \quad \pm\xi \quad 0), (0 \quad 0 \quad 0 \quad \pm\xi \quad \mp\xi \quad 0) \tag{25}$$

as the first two on the left yield the same value of P_6, whereas the last two give $-P_6$.

For completeness, here below we list the 12 strain vectors used to calculate the 5+10 independent SOECs and TOECs of a hexagonal material:

$$\begin{aligned}
&0 \rightarrow (0 \quad 0 \quad 0 \quad 0 \quad 0 \quad 0);\\
&1 \rightarrow (\pm\xi \quad 0 \quad 0 \quad 0 \quad 0 \quad 0);\\
&2 \rightarrow (0 \quad 0 \quad \pm\xi \quad 0 \quad 0 \quad 0);\\
&3 \rightarrow (0 \quad 0 \quad 0 \quad +\xi \quad 0 \quad 0);\\
&4 \rightarrow (\pm\xi \quad \pm\xi \quad 0 \quad 0 \quad 0 \quad 0), (\pm\xi \quad \mp\xi \quad 0 \quad 0 \quad 0 \quad 0);\\
&5 \rightarrow (0 \quad \pm\xi \quad 0 \quad 0 \quad 0 \quad 0);
\end{aligned} \tag{26}$$

where the two vectors labeled "1" allow to calculate $C_{11}^{(2)}$, $C_{12}^{(2)}$, $C_{13}^{(2)}$, $C_{111}^{(3)}$, $C_{112}^{(3)}$, and $C_{113}^{(3)}$; the two vectors labeled "2" yield $C_{33}^{(2)}$, $C_{333}^{(3)}$, and $C_{133}^{(3)}$; the vector labeled "3" allows to calculate $C_{44}^{(2)}$, $C_{144}^{(3)}$, $C_{155}^{(3)}$, and $C_{344}^{(3)}$; the four vectors labeled "4" yield $C_{123}^{(3)}$, and lastly, the two vectors labeled "5" allow to calculate $C_{222}^{(3)}$. Similar lists can be constructed for materials with the orthorhombic, monoclinic, and triclinic symmetry. In particular, it is easy to show that 10+8 deformed configurations (including reference state) are needed to calculate the 9+20 independent SOECs and TOECs of an orthorhombic material.

IV. COUPLING QHA WITH NONLINEAR CONTINUUM MECHANICS

Given a material in a selected reference state, the QHA method described in Sec. III can be used to calculate the total (static plus thermal) stress tensor, and the isochoric SOECs and TOECs at any temperature. These quantities can be used, in combination with Eqs. (8) and (11), to estimate changes in the lattice parameters occurring at a constant pressure and variable temperature, or at a constant temperature and variable pressure, as well as the SOECs of the material in any deformed configuration in a neighborhood of the reference state. These computationally inexpensive operations can be accomplished as follows.

To estimate the lattice parameters at, for example, zero pressure and increasing values of T, we use Eq. (8) to determine, the strain tensor, $\boldsymbol{\mu}(T)$, such that the PK2 tensor $\boldsymbol{P}(T, \boldsymbol{\mu})$ is equal to the null tensor. In general, to estimate the lattice parameters at selected values of p and T, the operations above can be outlined in the following schematic form:

$$\boldsymbol{V}, \boldsymbol{\sigma}, \boldsymbol{C}^{(2)}, \boldsymbol{C}^{(3)} \ldots \xrightarrow{\boldsymbol{\mu}(p,T)} \boldsymbol{P}(T, \boldsymbol{\mu}) \xrightarrow{\boldsymbol{F}} \boldsymbol{\sigma}(T, \boldsymbol{\mu}), \tag{27}$$

where $\boldsymbol{V}$ refers to the geometry of the reference state, and $\boldsymbol{\sigma}$, $\boldsymbol{C}^{(2)}$, and $\boldsymbol{C}^{(3)}$ are thermal stress tensor, and isochoric SOECs and TOECs calculated via QHA for the material in the reference state at the temperature T. These quantities are then plugged in Eq. (8) to determine via a numerical iterative procedure [56], the strain $\boldsymbol{\mu}(p, T)$ such that the PK2 stress, $\boldsymbol{P}(T, \boldsymbol{\mu})$, arising in the deformed configuration yields the desired Cauchy stress tensor, $\boldsymbol{\sigma}(T, \boldsymbol{\mu})$, at the desired temperature T. PK2 and Cauchy stresses are related to each other as in Eq. (11), where $\boldsymbol{F}$ is obtained from $\boldsymbol{\mu}(p, T)$ through inversion of Eq. (2) (see Sec. III B).

Given a pair of values p and T, the aforementioned procedure can be used to estimate the lattice parameters and geometry, $\tilde{\boldsymbol{V}}$, of a solid material whose isochoric thermoelastic parameters are are known only for a particular reference state. At this point, Eqs. (8) and (11) can again be combined to estimate the isothermal SOECs of the material in this new (deformed) configuration. To accomplish this task, we use the usual finite deformation approach, and therefore the finite difference formula in Eq. (17). In this case, however, for each deformed configuration of the reference state $\tilde{\boldsymbol{V}}$, the PK2 stress tensor is not calculated explicitly, but instead it is derived by combining Eqs. (8) and (11), as outlined in the following diagram:

$$\begin{aligned}
\tilde{\boldsymbol{V}} \xrightarrow{\tilde{\boldsymbol{\mu}}} \tilde{\boldsymbol{F}}, \tilde{\boldsymbol{V}}' \xrightarrow{\boldsymbol{V}} \boldsymbol{\mu}, \boldsymbol{F} \xrightarrow{\boldsymbol{\mu}} \boldsymbol{P}(T, \boldsymbol{\mu}) \xrightarrow{\boldsymbol{F}} \ldots\\
\ldots \xrightarrow{\boldsymbol{F}} \boldsymbol{\sigma}(T, \boldsymbol{\mu}) = \tilde{\boldsymbol{\sigma}}(T, \tilde{\boldsymbol{\mu}}) \xrightarrow{\tilde{\boldsymbol{F}}} \tilde{\boldsymbol{P}}(T, \tilde{\boldsymbol{\mu}}),
\end{aligned} \tag{28}$$

where $\tilde{\boldsymbol{F}}$ and $\tilde{\boldsymbol{\mu}}$ map the new reference state $\tilde{\boldsymbol{V}}$ to a deformed configuration $\tilde{\boldsymbol{V}}'$, $\boldsymbol{\mu}$ and $\boldsymbol{F}$ are the tensors mapping the original reference state $\boldsymbol{V}$ (for which thermal stress, and isothermal-isochoric SOECs and TOECs have been calculated explicitly) to $\tilde{\boldsymbol{V}}'$, and $\boldsymbol{P}(T, \boldsymbol{\mu})$ is the PK2 stress tensor of $\tilde{\boldsymbol{V}}'$ referred to the reference state $\boldsymbol{V}$, whereas $\tilde{\boldsymbol{P}}(T, \tilde{\boldsymbol{\mu}})$ is the PK2 tensor of $\tilde{\boldsymbol{V}}'$ referred to the deformed state $\tilde{\boldsymbol{V}}$.

As shown in the following sections, the aforementioned extrapolation techniques based on combining QHA and

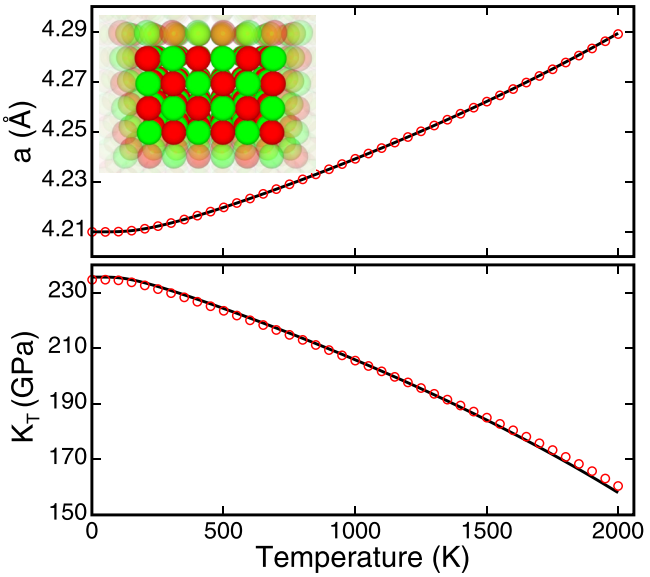

FIG. 2. Lattice parameter (top) and bulk modulus (bottom) of MgO vs T at zero pressure calculated by using a conventional QHA approach (red circles) and the methods presented in this work (black solid line), i.e., explicit QHA calculation of thermal stress, isochoric-isothermal SOECs and TOECs for a reference state yielding a zero static pressure, followed by the extrapolation procedure described in Sec. IV. MgO is described through the use cubic supercells contains 512 (red circles) and 64 (black solid line) atoms. Inset, rock-salt structure of MgO.

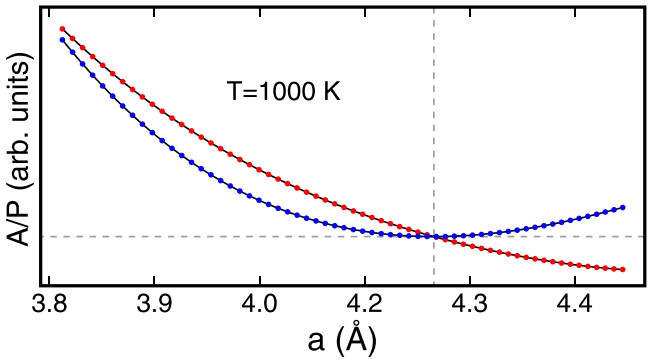

FIG. 3. Helmholtz free energy (blue discs) and pressure (red discs) vs the lattice parameter of MgO at 1000 K. Symbols show results calculated as described in the text by using an energy scheme based on classical interatomic potentials [50], whereas solid black curves are the result of a polynomial interpolation.

nonlinear continuum mechanics yield accurate results of lattice parameters and isothermal SOECs within intervals of temperature and pressure inducing deformations of the reference state, $\boldsymbol{V}$, of a few percents in strain. Needless to say, these extrapolation techniques can be applied to obtain a thermoelastic characterization of a material in a neighborhood of a reference state wherein electronic or ionic phase transitions are absent.

V. METHODS VALIDATION

To demonstrate validity and assess limitations of our methods, we carry out rigid-ion atomistic calculations of MgO using the Born-Mayer interatomic potentials of Ref. [50]. We use a proprietary code [57] to run these calculations. This code implements the Ewald method to calculate electrostatic energy and forces, a damped molecular dynamics approach to optimize ionic positions, and the small displacement method to calculate phonon frequencies and normal modes at Γ. The results of combining our new methods with this type of calculations are shown in Figs. 2–5.

Figure 2 shows the lattice parameter and bulk modulus of MgO versus T calculated by using both the present methods (Secs. III and IV) and a conventional QHA approach [32,34–42]. In this latter type of calculations, we use a grid of cubic supercells of MgO, obtained by applying a hydrostatic strain ranging from −0.0875 to 0.0625 at intervals of 0.0025 to a reference state yielding a zero static pressure. For each volume, we calculate phonon frequencies, harmonic Helmholtz free energy [Eq. (12)], as well as the isotropic mode Grüneisen parameters and hence total stress tensor [Eq. (13)] by using both the conventional technique based on Eq. (14) and the recently proposed approach relying on Eqs. (15) and (16) [54]. At each T, we then use a seventh-order polynomial to interpolate both the free energy and the pressure values (Fig. 3), which are used separately to derive the values of lattice parameter and bulk modulus, at a zero or finite external pressure. As expected, these redundant calculations show that, indeed, our QHA method (relying the use of the stress tensor and a novel approach to calculate generalized mode Grüneisen parameters [54]) gives the same results as the conventional QHA approach (based on the use of the free energy). Furthermore, we repeated these QHA calculations by employing cubic supercells containing 64, 216, and 512 atoms, obtaining very similar results. This shows that to obtain converged results, our QHA method requires the use of nonprimitive supercells containing >64 atoms, i.e., a few hundreds or more normal modes at Γ.

Figures 2 and 4 show also the results obtained by combining our QHA method with nonlinear continuum mechanics (Sec. IV). In particular, Fig. 4 shows values of SOECs calculated explicitly at selected temperatures by using our QHA approach (Sec. III), compared to values obtained by employing our strategy based on combining QHA with nonlinear continuum mechanics (Sec. IV). In these latter calculations, both lattice parameter (Fig. 2) and isothermal SOECs at zero pressure (Fig. 4) are extrapolated by using values of thermal stress (Eq. (13)), and isochoric-isothermal SOECs and TOECs calculated explicitly via QHA for a reference state yielding a zero static pressure. Also in this case, calculations carried out by using supercells containing 64, 216, and 512 atoms give equivalent results.

Overall, the results and comparisons in Figs. 2 and 4 show that, the present implementation of QHA (relying on a new method to calculate generalized mode Grüneisen parameters [54] and the use of the stress tensor to calculate isothermal SOECs and TOECs of a solid material at constant volume) yields results equivalent to those obtained from a conventional QHA approach relying on the Helmholtz free energy to calculate thermoelastic parameters. Furthermore, our calculations demonstrate that the combination of our QHA approach with

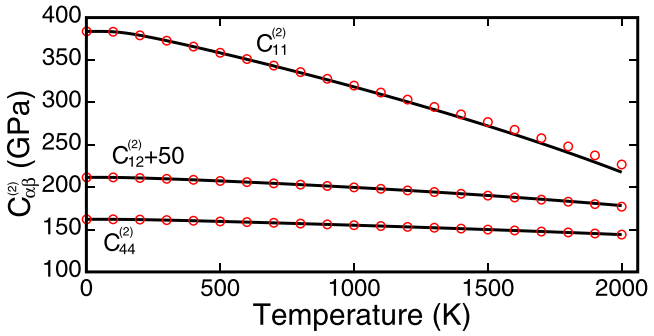

FIG. 4. Isothermal SOECs of MgO at zero pressure vs T calculated by using the present methods. Red circles show results obtained by calculating SOECs explicitly through the use of our implementation of QHA; at each T, we used our QHA method to calculate the isothermal-isochoric SOECs of MgO with lattice parameter $a(T)$ (Fig. 2). The black solid lines show values of SOECs obtained by using the extrapolation procedure relying on nonlinear continuum mechanics discussed in Sec. IV, using thermal stress, SOECs and TOECs calculated explicitly via QHA for a reference state yielding a zero static pressure.

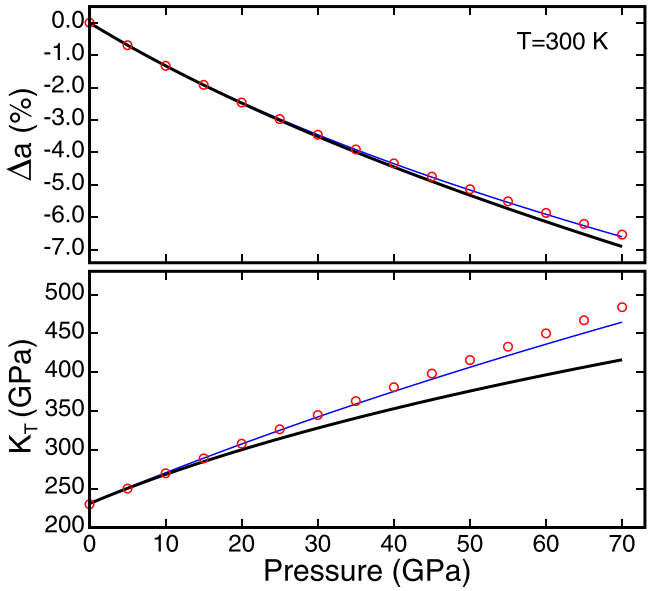

FIG. 5. Percent variation of the lattice parameter (top) and bulk modulus (bottom) of MgO at 300 K vs pressure calculated by using a conventional QHA approach (red circles) and the methods presented in this work (solid lines), i.e., explicit calculation by using our QHA method of thermal stress, and isochoric-isothermal linear and nonlinear elastic constants for a reference state yielding a zero static pressure, followed by the extrapolation procedures relying on nonlinear continuum mechanics described in Sec. IV. The black solid line shows results obtained by combining Eqs. (8) and (11), whereas the thin blue solid line shows results obtained by including in Eq. (8) also the leading third-order terms in strain [Eq. (29)], whose coefficients are the isothermal-isochoric fourth-order elastic constants $C^{(4)}_{\alpha\beta\beta\beta}$, with $\alpha, \beta = 1, \ldots, 6$.

nonlinear continuum mechanics allows to obtain a thermoelastic characterization of a solid material in a neighborhood of a reference state, and thus to estimate lattice parameters and isothermal SOECs over meaningful intervals of temperature and pressure. This is clearly shown in Fig. 5, showing values of lattice parameter and bulk modulus of MgO at 300 K and pressures ranging from 0 to 70 GPa, as obtained by using both conventional QHA calculations and the present methods. These results show that the extrapolation technique relying on Eqs. (8) and (11) yields meaningful and reliable results for both the lattice constant and bulk modulus up to a strain of about 2%. Interestingly, this interval can be extended up to a strain of about 6%, by accounting in Eq. (8) also for the leading third-order terms in strain, as follows:

$$P_\alpha(\boldsymbol{\mu}) = C^{(1)}_\alpha + C^{(2)}_{\alpha\beta}\mu_\beta + \tfrac{1}{2}C^{(3)}_{\alpha\beta\gamma}\mu_\beta\mu_\gamma + \tfrac{1}{6}C^{(4)}_{\alpha\beta\beta\beta}\mu_\beta^3, \quad (29)$$

where the fourth-order elastic constants $C^{(4)}_{\alpha\beta\beta\beta}$ can be obtained by using the following finite-difference formula:

$$C^{(4)}_{\alpha\beta\beta\beta} = \frac{\partial^3 P_\alpha}{\partial {\mu_\beta}^3} \approx \frac{P_\alpha^{(+2\Delta\mu_\beta)} - 2P_\alpha^{(\Delta\mu_\beta)} + 2P_\alpha^{(-\Delta\mu_\beta)} - P_\alpha^{(-2\Delta\mu_\beta)}}{2{\Delta\mu_\beta}^3}. \quad (30)$$

VI. APPLICATIONS

Our methods in combination with a DFT approach are used to calculate selected thermoelastic properties of silicon, lithium hydride, and graphite. These calculations are carried out using the QUANTUM ESPRESSO package [51,52] and pseudopotentials from the PSLIBRARY [58].

A. Technical details of DFT calculations

To describe the diamond structure of Si, we use an ultrasoft pseudopotential, *Si.pz-nl-rrkjus_psl.1.0.0.UPF*, a local density approximation (LDA) functional [59], and plane-wave energy cutoffs of 44 and 176 Ry for wave functions and electron charge density, respectively. We use a uniform mesh of $8 \times 8 \times 8$ $\boldsymbol{k}$ points to sample the Brillouin zone of primitive unit cells, whereas we employ a grid of $2 \times 2 \times 2\boldsymbol{k}$ points and the Γ point to sample the Brillouin zones of the nonprimitive cubic supercells containing 64 and 216 Si atoms, respectively. To describe the rock-salt structure of LiH, we use a generalized gradient approximation (GGA) functional [60], the pseudopotentials *Li.pbe-sl-rrkjus_psl.1.0.0.UPF* and *H.pbe-rrkjus_psl.1.0.0.UPF*, and plane-wave energy cutoffs of 50 and 325 Ry. We use a uniform mesh of $10 \times 10 \times 10$ $\boldsymbol{k}$ points to sample the Brillouin zone of primitive unit cells, and uniform meshes of $3 \times 3 \times 3$ and $2 \times 2 \times 2$ $\boldsymbol{k}$-points in case of cubic supercells containing 64 and 216 atoms, respectively. To describe AB-stacked hexagonal structure of graphite, we use a GGA functional [61], the pseudopotential *C.pbesol-n-rrkjus_psl.1.0.0.UPF*, and plane-wave cutoff energies equal to 80 and 550 Ry. We use a uniform mesh of $10 \times 10 \times 4\boldsymbol{k}$ points to sample the Brillouin zone of primitive unit cells of LiH, and a grid of $4 \times 4 \times 2$ $\boldsymbol{k}$ points to sample the Brillouin zone of a hexagonal supercell containing $5 \times 5 \times 1$ unit cells and a total of 100 C atoms.

We use the finite displacement method to calculate Γ-point phonon frequencies of solids described by the use of nonprimitive supercells, whereas we rely on density functional perturbation theory (DFPT) [51,52,62] to calculate harmonic

TABLE I. Lattice parameters (in angstroms) and SOECs (in GPa) of Si, LiH, and graphite calculated by using the present methods and DFT calculations. For each material, the first row shows results obtained in static conditions, that is at 0 K and in absence of zero-point quantum corrections. The second row shows results at 0 K accounting for zero-point quantum corrections. The third and fourth rows show values of lattice parameters and SOECs at a zero total pressure and temperatures of 0 and 300 K, respectively. These results are obtained by using the extrapolation procedure in Sec. IV, by employing the isothermal-isochoric SOECs and TOECs calculated via our QHA method for the reference state in the first row. Experimental data obtained at room temperature are also shown for comparison.

T (K)	p (GPa)	a_0	c_0	$C^{(2)}_{11}$	$C^{(2)}_{12}$	$C^{(2)}_{44}$	$C^{(2)}_{13}$	$C^{(2)}_{33}$
Silicon								
–	−0.34	5.409	–	160	64	76	–	–
0	0.11	5.409	–	159	64	75	–	–
0	0.00	5.411	–	158	64	75	–	–
300	0.00	5.412	–	156	62	74	–	–
Refs. [63,64]		5.431	–	166	64	80	–	–
Lithium hydride								
–	−2.02	4.090	–	65	13	43	–	–
0	0.03	4.090	–	68	14	43	–	–
0	0.00	4.092	–	67	14	43	–	–
300	0.00	4.115	–	56	15	44	–	–
Refs. [65,66]		4.084	–	67	15	46	–	–
Graphite								
–	0.00	2.459	6.695	1086	208	5	−2	31
0	2.51	2.459	6.695	1085	209	5	−2	32
0	0.00	2.466	6.719	1056	199	4	−2	30
300	0.00	2.465	6.763	1037	191	4	0	27
Ref. [67]		2.463	6.712	1109	139	5	0	39

frequencies of solids described by the use of primitive unit cells. In this latter case, we use DFPT to calculate dynamical matrices on a $4 \times 4 \times 4$ uniform grid of $\boldsymbol{q}$ points in the Brilouin zone, followed by an inverse Fourier transform to obtain real-space interatomic force constants, and Fourier interpolation to estimate dynamical matrices and frequencies on a $10 \times 10 \times 10$ grid of $\boldsymbol{q}$ points.

B. Results and discussion

Table I reports lattice parameters and SOECs of Si, LiH, and graphite in static conditions in selected reference states, and at zero pressure and temperatures of 0 and 300 K. These latter results are obtained by using our strategy based on combining QHA and nonlinear continuum mechanics, as described in Sec. IV. We remark that results obtained in static conditions agree well with previous DFT studies [42,68–70], and that our results at 300 K are within the expected level of agreement with the experimental data (Table I). The Debye temperatures of Si, LiH, and graphite are larger than 300 K, and therefore QHA is expected to yield satisfactory results at this temperature for these three materials. We can then conclude that the small differences between calculated and experimental data at 300 K are attributed to limits of the DFT approach (based on the use of pseudopotentials and approximations of the exchange-correlation energy), rather than deficiencies of QHA. It is also interesting to note that lattice parameters and SOECs at 300 K exhibit small although noticeable deviations from the values obtained in static conditions. This demonstrates the well-established notion that quantum motion and anharmonic effects influence the properties of a material, and that although QHA accounts only in part for anharmonic effects, it can nonetheless be used to achieve a meaningful description of a broad class of materials over finite intervals of temperature and pressure.

TABLE II. TOECs (in GPa) of Si calculated by using a DFT approach and the methods presented in Sec. III. TOECs at zero temperature are calculated for increasing values of the strain parameter ξ; TOECs obtained by using Eq. (19) are indicated with a tilde. The fourth from the last row reports TOECs at 300 K calculated by using our QHA method and $\xi = 0.0100$. All these TOECs are calculated for a reference state yielding a static pressure of −0.34 GPa. The last three rows report experimental values of TOECs measured at room temperature.

ξ	$C^{(3)}_{111}$	$C^{(3)}_{211}$	$\tilde{C}^{(3)}_{112}$	$C^{(3)}_{144}$	$\tilde{C}^{(3)}_{441}$	$C^{(3)}_{155}$	$\tilde{C}^{(3)}_{551}$	$\tilde{C}^{(3)}_{123}$	$\tilde{C}^{(3)}_{456}$
0.0025	−764	−456	−451	31	37	−292	−299	−87	−52
0.0050	−759	−454	−454	31	31	−296	−296	−85	−52
0.0075	−761	−453	−453	29	30	−296	−295	−85	−52
0.0100	−761	−453	−453	27	28	−295	−295	−84	−52
0.0125	−761	−453	−453	28	28	−295	−295	−85	−53
0.0150	−761	−454	−453	28	28	−295	−295	−85	−53
0.0100	−710	−443	–	44	–	−271	–	−70	−45
Ref. [64]	−795	−445	–	15	–	−310	–	−75	−86
Ref. [23]	−825	−451	–	12	–	−310	–	−64	−64
Ref. [27]	−817	−493	–	−25	–	−293	–	−192	−37

Tables II and III report values of TOECs for silicon and graphite calculated as discussed in Sec. III, by using a DFT approach, Eqs. (17)–(19), and the lists of deformations in (23) and (26), respectively. TOECs at 0 K are calculated by using a strain parameter ξ ranging from 0.0025 to 0.0150, primitive unit cells, and stringent convergence criteria

TABLE III. TOECs (in GPa) of graphite calculated by using a DFT approach and the methods presented in Sec. III. TOECs are calculated in static conditions for a reference state yielding zero static pressure and increasing values of the strain parameter ξ. The last column reports TOECs at 300 K and zero total pressure calculated by using our QHA method and $\xi = 0.0100$.

ξ	0.0025	0.0050	0.0075	0.0100	0.0125	0.0150	0.0100
$C^{(3)}_{111}$	−9591	−9606	−9602	−9616	−9629	−9642	−8487
$C^{(3)}_{222}$	−8916	−8873	−8956	−8956	−8962	−8966	−7784
$C^{(3)}_{333}$	−594	−595	−604	−598	−604	−610	−647
$C^{(3)}_{211}$	−1411	−1391	−1403	−1396	−1392	−1388	−1003
$C^{(3)}_{311}$	19	31	31	29	29	29	−96
$C^{(3)}_{133}$	35	25	23	24	24	23	−82
$C^{(3)}_{144}$	0	−2	−1	−1	−2	−2	−2
$C^{(3)}_{155}$	7	11	8	8	9	9	−4
$C^{(3)}_{344}$	−72	−83	−82	−82	−83	−82	−84
$C^{(3)}_{123}$	−53	−63	−85	−63	−76	−68	−82

(threshold on forces and selfconsistency equal to 10^{-6} and 10^{-15} a.u., respectively) [55]. TOECs at 300 K and zero pressure are calculated by using our novel implementation of QHA (Sec. III) and supercells containing 216 and 100 Si and C atoms, respectively.

The results in Tables II and III show that Eqs. (18) and (19) give results that depend little on the value of the strain parameter (ξ). In particular, Table II shows that equivalent TOECs, such as $C^{(3)}_{144}$ and $C^{(3)}_{441}$, can be calculated by using either Eq. (18) or Eq. (19). These two finite difference equations yield very similar results, with small differences originating from truncation errors, which are inherently different for these two formulas. Table II reports also TOECs of Si at 300 K and a total pressure of 0.11 GPa (Table I) calculated by using our QHA approach. We remark that our values compare well with experimental TOECs measured at room temperature [23,27,64] (Table I). Also in this case, considering the harmonic nature of Si and the values of the temperature and pressure, it is reasonable to conclude that the small differences between calculated and experimental data are attributed to limits of our DFT approach. The investigation of these issues lies outside the scope of the present work.

Table III reports values of TOECs at 300 K and zero pressure calculated by using our QHA approach. These values are in good agreement with TOECs calculated by using a anharmonic Keating model for graphite [71]. To the best of our knowledge, the present work is the first one reporting TOECs of graphite calculated from first principles, whereas only one recent experimental effort was undertaken to measure selected nonlinear elastic constants of this material [72]. Unfortunately, these measurements led to contradicting results, most likely due to both the lack of crystallinity and the different microstructural properties of the graphite samples used in the experiments [72]. For example, in this experimental work $C^{(3)}_{111}$ was found to be equal to -120 GPa in case of isostatic graphite (an isotropic, high-density, fine-grained form of graphite), and equal to 377 and -203 GPa in case of graphite samples obtained by cold pressing of graphite powder from low-ash petroleum coke [72].

Figure 6 shows the lattice parameter, the linear thermal expansion coefficient, and bulk modulus of Si at zero pressure and temperatures up to 1500 K. These results are obtained by using both the methods presented in this work and a conventional QHA approach. In particular, in these latter calculations we use primitive unit cells, a DFPT approach to calculate phonon frequencies, and lattice parameter and bulk modulus are obtained from the first- and second-order derivatives of the Helmholtz free energy with respect to volume, respectively. To calculate the same quantities, we use the approach combining results obtained from QHA with nonlinear continuum mechanics (Sec. IV). In detail, we use our QHA method to calculate total stress, and isothermal-isochoric SOECs and TOECs for a reference state yielding a static pressure of -0.34 GPa at 0 K (Table I). Then, we employ the extrapolation procedures described in Sec. IV to calculate lattice parameters, SOECs and elastic moduli at zero pressure and increasing temperature. These calculations are repeated by using cubic supercells containing 64 and 216 Si atoms.

Figure 6 shows that our results are in excellent agreement with those obtained by using a conventional QHA approach.

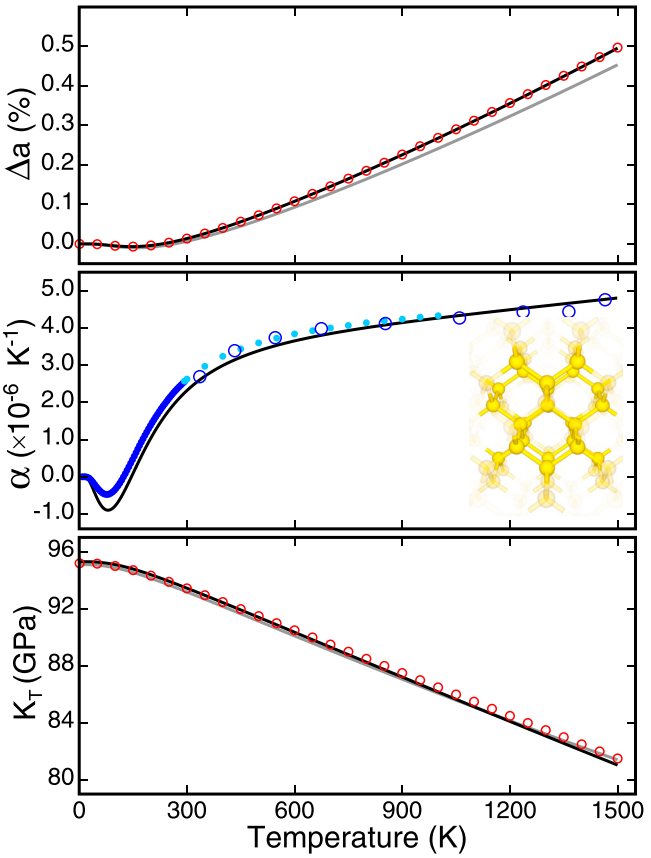

FIG. 6. Percent variation of the lattice parameter (top), linear thermal expansion coefficient (middle), and bulk modulus (bottom) of Si at zero pressure and increasing T. Solid lines show results obtained from DFT by employing supercells containing 64 (gray) and 216 (black) atoms, and by carrying out QHA calculations of thermal stress, and isothermal-isochoric SOECs and TOECs for a reference state yielding a static pressure of -0.34 GPa, followed by the extrapolation technique discussed in Sec. IV. Red circles show results obtained by using a conventional QHA approach [42]. Experimental data for the linear thermal expansion coefficient are from Refs. [74] (blue discs), and [75] (light blue discs), and [27] (blue circles). Inset, the diamond structure of Si.

As expected, Fig. 6 shows also that, although results obtained by using the smaller supercell are satisfactory, a better agreement and full convergence are obtained when a larger supercell containing 216 Si atoms is used. These results demonstrate that our methods are sound and that to achieve convergence, our methods require the use of supercells containing about a hundred or more atoms, or equivalently, a supercell sufficiently large to accommodate a few hundreds or more normal modes at the Γ point. We also remark that the results in Fig. 6 are in excellent agreement with recent QHA studies of Si [42], and that calculated and experimental values of the linear thermal expansion coefficient (Fig. 6) show the expected level of agreement [73].

Figure 7 shows the lattice parameter of LiH at zero pressure and temperatures up to 300 K, and at 300 K and external pressures ranging from 0 up to 40 GPa. In Fig. 7, results obtained by using both our methods and conventional QHA calculations are compared to selected experimental data [65,76]. In

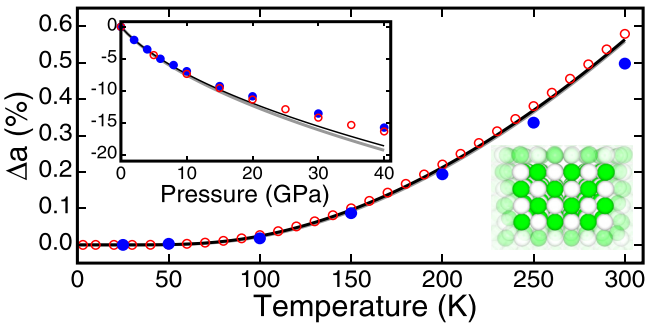

FIG. 7. Percent variation of the lattice constant of LiH vs T at zero pressure, and (inset, top left) vs pressure at 300 K, calculated by using both a conventional QHA approach (solid red circles) and our methods. Gray and black solid lines show results obtained by using supercells containing 64 and 216 atoms, respectively. Blue discs show selected experimental data extracted from Refs. [65,76]. Inset, bottom right, the rock-salt structure of LiH.

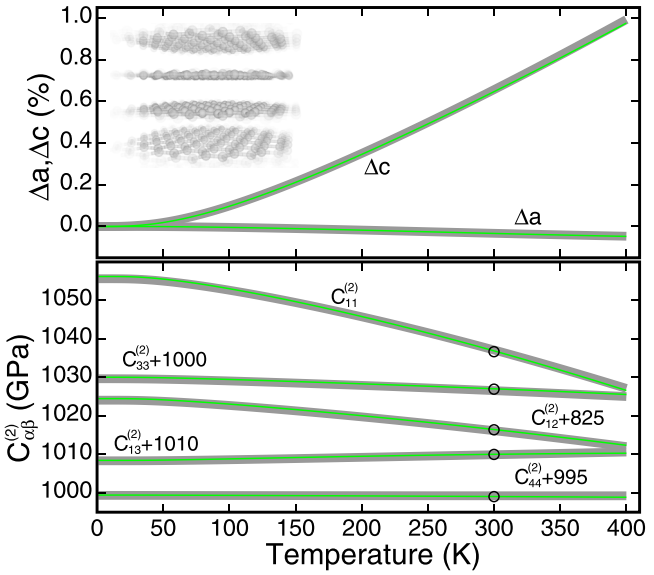

FIG. 8. (Top) Percent variation of the in-plane (a) and out-of-plane (c) lattice parameters of graphite vs T. Bottom panel, independent SOECs of graphite vs T; values are shifted as indicated in figure. These results are obtained from DFT by using our QHA method to calculate thermal stress, SOECs and TOECs for a reference state, followed by the use of the extrapolation techniques relying on nonlinear continuum mechanics discussed in Sec. IV. Thick gray curves show results obtained by considering a reference state yielding a zero static pressure at 0 K, whereas the solid green lines show results obtained by considering a reference state yielding a zero total pressure at 300 K. DFT calculations are carried out by using a hexagonal supercell containing 100 atoms, consisting of a $5 \times 5 \times 1$ array of primitive unit cells. Inset, top left corner, an image showing the layered structure of graphite.

particular, we use primitive unit cells in the conventional QHA calculations, whereas we use cubic supercells containing 64 and 216 to calculate the isothermal-isochoric SOECs and TOECs by using our QHA approach. These latter quantities, calculated for a reference state yielding a static pressure of −2.020 GPa (Table I), are then used in combination with the extrapolation procedures of Sec. IV to estimate the lattice parameter of LiH at finite temperature and pressure.

Our calculations (Fig. 7) show that results obtained by using the present methods are in overall good agreement with both experimental data and conventional QHA. Figure 7 shows also that, as expected, our extrapolation technique gradually loses accuracy as the deformed state for which predictions are sought falls farther away, in terms of strain, from the reference state. We remark that our DFT calculations give a lattice parameter of LiH in static conditions and zero pressure equal to 4.006 Å, that is ∼2% smaller than the value of LiH in the reference state used to derive the results in Table I and Fig. 7. Although, for convenience, we opted to use this latter configuration as reference state to extrapolate all the results in Fig. 7, we can state that the use of the former configuration as reference state (of another one with a smaller lattice parameter) would yield results of Δa at 300 K and increasing pressure agreeing with conventional QHA over a wider interval of pressures.

To demonstrate merits and further corroborate validity of our methods, we consider the case of graphite, a hexagonal material exhibiting strong anisotropy in the structural, and hence, thermoelastic properties. In detail, we use our QHA method to calculate isothermal-isochoric SOECs and TOECs of graphite in two different reference states: (i) the configuration with a zero static pressure at 0 K, and (ii) a state having a zero total (static plus thermal) pressure at 300 K (Table I). Then, we use the SOECs and TOECs of these two reference states, combined with the extrapolation procedures described in Sec. IV, to estimate lattice parameters and SOECs at zero pressure and at temperatures from 0 to 400 K. Figure 8 shows that these two sets of calculations produce identical results, and hence that SOECs of graphite at 300 K can be determined explicitly via DFT by using our QHA method, or via extrapolation by using SOECs and TOECs calculated via DFT and our QHA method for a reference state yielding a zero static pressure. For completeness, in Fig. 9, we show the linear thermal expansion coefficients of graphite obtained from our approach combining QHA calculations and nonlinear continuum mechanics. These results compare well with experimental data [77]. Overall, this last application shows that our methods are suited to investigate the thermoelastic properties of materials of any symmetry and the combination of our QHA method with nonlinear continuum mechanics consists of an efficient computational strategy to calculated lattice parameters and SOECs over meaningful intervals of temperature and pressure.

VII. CONCLUSION AND OUTLOOK

In this work, we have introduced a novel implementation of QHA to calculate from first principles both SOECs and, most notably, TOECs of a material at finite temperature and constant volume. This method relies on finite deformations and the numerical differentiation of the (second Piola-Kirchhoff) stress tensor to calculate both SOECs and TOECs [55], and it employs a recently proposed method [54] to calculate generalized mode Grüneisen parameters and hence stress tensor. Thanks to this, the present QHA method involves a

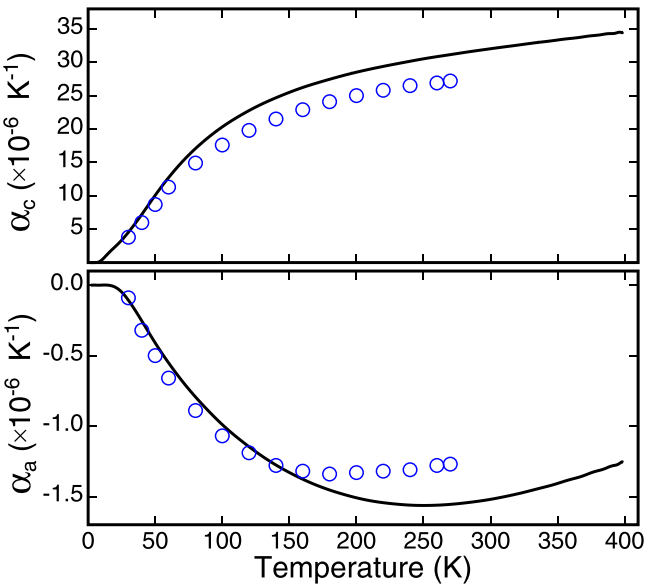

FIG. 9. Linear thermal expansion coefficients parallel (top) and perpendicular (bottom) to the c axis of graphite. Black solid lines show results obtained by combining QHA calculations and nonlinear continuum mechanics, whereas blue circles show experimental data [77].

manageable computational workflow that, measured in terms of number of deformed configurations, requires only 4, 6, and 10 configurations (including reference state) to calculate the SOECs of a material with the cubic, hexagonal, and orthorhombic symmetry, respectively. These numbers increase to 8, 12, and 18 to obtain the 6, 10, and 20 independent TOECs of a material with the cubic, hexagonal, and orthorhombic symmetry, respectively. The main disadvantage of the present QHA implementation is that it requires the use of large nonprimitive supercells, containing a sufficient number of atoms, and hence normal modes at Γ, to obtain converged values of the thermal stress tensor, and hence SOECs and TOECs.

In this work, we have also introduced a computational strategy combining QHA calculations and elementary equations of nonlinear continuum mechanics. This hybrid approach allows to estimate thermoelastic parameters over finite intervals of temperature and pressure, at the cost of calculating via QHA the isothermal-ishochoric SOECs and TOECs of a material in an opportune reference state. Here, both our novel implementation of QHA and the computational strategy relying on nonlinear continuum mechanics have been used to calculate selected thermoelastic properties of Si, LiH, and graphite. Our results show that our QHA implementation yields results equivalent to those obtained by using a conventional QHA approach. Furthermore, they show that the computational strategy combining QHA calculations and nonlinear continuum mechanics yields accurate predictions of thermoelastic properties for configurations of a material that are within about $\pm 1\%$ in strain from a reference state (whose SOECs and TOECs have been calculated explicitely via QHA). This strain interval translates into meaningful intervals of temperature and pressure.

Overall, taking into account both advantages and disadvantages, we envision that the methods presented in this work have the potential to be used for the following purposes. One, the calculation from first principles of nonlinear elastic constants (TOECs and potentially fourth-order elastic constants) of materials at finite temperature through the use of our QHA method. TOECs are important coefficients characterizing the nonlinear mechanical response of a material subjected to a deformation, and thereby related to properties such as sound attenuation and yield strength [55]. Our QHA method can be used to calculate these nonlinear elastic coefficients at finite temperature for a variety of materials, for which experimental data are still missing or difficult to obtain, as in case of graphite. Two, the calculation from first principles of isothermal SOECs of materials with the orthorhombic, monoclinic, or triclinic symmetry, classes of materials that is within the reach of our QHA approach. We remark that our QHA approach requires the same minimal list of configurations, that is 9 deformed states plus reference state, to calculate the 9, 13, and 21 independent SOECs of materials with the orthorhombic, monoclinic, or triclinic symmetry, respectively. This puts our implementation of QHA at the forefront, together with other well-established techniques [36,41,45,49,78], to study thermoelastic properties of low-symmetry solids. Three, the calculation from first principles of thermal expansion coefficients and SOECs of a material over finite intervals of temperature and pressure through the use of our approach combining QHA calculations and nonlinear continuum mechanics. We underline that this approach is computationally efficient, as it involves only the calculation of the isothermal-isochoric SOECs and TOECs via QHA for a single reference state. We also remark that this approach is applicable to materials of arbitrary symmetry and complexity, and therefore it could be used to build databases of materials properties at finite temperature [29,32], or investigate the thermoelastic and mechanical properties of, for example, minerals of geological relevance [30,36,78,79] or metal alloys for structural applications [12–16,80].

ACKNOWLEDGMENTS

This work is supported by the National Science Foundation (NSF), Award No. DMR-2036176. We acknowledge the support of the CUNY High Performance Computing Center, the PSC-CUNY Grants No. 62651-0050 and No. 63913-0051.

[1] O. L. Anderson, *Equation of State of Solids for Geophysics and Ceramic Science* (Oxford University Press, New York, 1995).

[2] J. Clayton, *Nonlinear Mechanics of Crystals* (Springer, Dordrecht, 2011), Vol. 177.

[3] J. D. James, J. A. Spittle, S. G. R. Brown, and R. W. Evans, Meas. Sci. Technol. **12**, R1 (2001).

[4] P. G. Klemens, Int. J. Thermophys. **9**, 171 (1988).

[5] O. L. Anderson and D. G. Isaak, *Elastic Constants of Mantle Minerals at High Temperature* (American Geophysical Union (AGU), Washington, DC, 1995), pp. 64–97.

[6] A. Yeganeh-Haeri, D. J. Weidner, and E. Ito, Science **243**, 787 (1989).

[7] T. B. Ballaran, A. Kurnosov, K. Glazyrin, D. J. Frost, M. Merlini, M. Hanfland, and R. Caracas, Earth Planet. Sci. Lett. **333–334**, 181 (2012).
[8] C. Varvenne, A. Luque, and W. A. Curtin, Acta Mater. **118**, 164 (2016).
[9] C. Varvenne, G. Leyson, M. Ghazisaeidi, and W. Curtin, Acta Mater. **124**, 660 (2017).
[10] H. Wang and M. Li, Phys. Rev. B **85**, 104103 (2012).
[11] B. Yin and W. A. Curtin, npj Comput. Mater. **5**, 14 (2019).
[12] C. R. Krenn, D. Roundy, M. L. Cohen, D. C. Chrzan, and J. W. Morris, Phys. Rev. B **65**, 134111 (2002).
[13] L. Qi and D. C. Chrzan, Phys. Rev. Lett. **112**, 115503 (2014).
[14] I. S. Winter, M. de Jong, M. Asta, and D. C. Chrzan, Phys. Rev. Materials **1**, 030601(R) (2017).
[15] M. de Jong, I. Winter, D. C. Chrzan, and M. Asta, Phys. Rev. B **96**, 014105 (2017).
[16] I. S. Winter, M. de Jong, J. Montoya, E. Rothchild, and D. C. Chrzan, Phys. Rev. Materials **3**, 113608 (2019).
[17] G. A. Saunders, Phys. Scr. **1982**, 49 (1982).
[18] M. A. Carpenter and E. K. H. Salje, Eur. J. Mineral. **10**, 693 (1998).
[19] P. Toledano, M. M. Fejer, and B. A. Auld, Phys. Rev. B **27**, 5717 (1983).
[20] H. Babaei and V. I. Levitas, Phys. Rev. Lett. **124**, 075701 (2020).
[21] R. Thurston and K. Brugger, Phys. Rev. **133**, A1604 (1964).
[22] G. B. Benedek and K. Fritsch, Phys. Rev. **149**, 647 (1966).
[23] H. J. McSkimin and P. Andreatch, J. Appl. Phys. **35**, 2161 (1964).
[24] H. J. McSkimin, P. Andreatcah, and N. T. Thurston, J. Appl. Phys. **36**, 1624 (1965).
[25] N. T. Thurston, H. J. McSkimin, and P. Andreatch, J. Appl. Phys. **37**, 267 (1966).
[26] H. J. McSkimin and P. Andreatch, J. Appl. Phys. **43**, 2944 (1972).
[27] J. Philip and M. A. Breazeale, J. Appl. Phys. **54**, 752 (1983).
[28] A. S. Johal and D. J. Dunstan, Phys. Rev. B **73**, 024106 (2006).
[29] M. de Jong, W. Chen, T. Angsten, A. Jain, R. Notestine, A. Gamst, M. Sluiter, C. K. Ande, S. van der Zwaag, J. J. Plata, *et al.*, Sci. Data **2**, 150009 (2015).
[30] A. Kurnosov, H. Marquardt, D. J. Frost, T. B. Ballaran, and L. Ziberna, Nature (London) **543**, 543 (2017).
[31] J.-F. Lin, Z. Mao, J. Yang, and S. Fu, Nature (London) **564**, E18 (2018).
[32] P. Nath, J. J. Plata, D. Usanmaz, R. Al Rahal Al Orabi, M. Fornari, M. B. Nardelli, C. Toher, and S. Curtarolo, Comput. Mater. Sci. **125**, 82 (2016).
[33] A. Erba, M. Shahrokhi, R. Moradian, and R. Dovesi, J. Chem. Phys. **142**, 044114 (2015).
[34] B. B. Karki, R. M. Wentzcovitch, S. de Gironcoli, and S. Baroni, Science **286**, 1705 (1999).
[35] B. B. Karki, R. M. Wentzcovitch, S. de Gironcoli, and S. Baroni, Phys. Rev. B **61**, 8793 (2000).
[36] R. M. Wentzcovitch, B. B. Karki, M. Cococcioni, and S. de Gironcoli, Phys. Rev. Lett. **92**, 018501 (2004).
[37] N. Mounet and N. Marzari, Phys. Rev. B **71**, 205214 (2005).
[38] M. Núñez Valdez, K. Umemoto, and R. M. Wentzcovitch, Appl. Phys. Lett. **101**, 171902 (2012).
[39] E. T. Ritz, S. J. Li, and N. A. Benedek, J. Appl. Phys. **126**, 171102 (2019).
[40] H. H. Pham, M. E. Williams, P. Mahaffey, M. Radovic, R. Arroyave, and T. Cagin, Phys. Rev. B **84**, 064101 (2011).
[41] Z. Wu and R. M. Wentzcovitch, Phys. Rev. B **83**, 184115 (2011).
[42] C. Malica and A. D. Corso, J. Phys.: Condens. Matter **32**, 315902 (2020).
[43] A. Oganov, in *Treatise on Geophysics*, edited by G. Schubert (Elsevier, Amsterdam, 2007), pp. 121–152.
[44] A. R. Oganov and P. I. Dorogokupets, Phys. Rev. B **67**, 224110 (2003).
[45] Z. Zhang and R. M. Wentzcovitch, Phys. Rev. B **103**, 104108 (2021).
[46] F. D. Murnaghan, Proc. Natl. Acad. Sci. U.S.A. **30**, 244 (1944).
[47] P. Vinet, J. Ferrante, J. R. Smith, and J. H. Rose, J. Phys.: Solid State Phys. **19**, L467 (1986).
[48] M. Palumbo and A. D. Corso, J. Phys.: Condens. Matter **29**, 395401 (2017).
[49] C. K. Gan and K. T. E. Chua, J. Phys.: Condens. Matter **31**, 265401 (2019).
[50] G. V. Lewis, Physica B+C **131**, 114 (1985).
[51] P. Giannozzi, S. Baroni, N. Bonini, M. Calandra, R. Car, C. Cavazzoni, D. Ceresoli, G. L. Chiarotti, M. Cococcioni, I. Dabo *et al.*, J. Phys.: Condens. Matter **21**, 395502 (2009).
[52] P. Giannozzi, O. Andreussi, T. Brumme, O. Bunau, M. B. Nardelli, M. Calandra, R. Car, C. Cavazzoni, D. Ceresoli, M. Cococcioni *et al.*, J. Phys.: Condens. Matter **29**, 465901 (2017).
[53] D. C. Wallace, Phys. Rev. **162**, 776 (1967).
[54] D. Cuffari and A. Bongiorno, Phys. Rev. Lett. **124**, 215501 (2020).
[55] T. Cao, D. Cuffari, and A. Bongiorno, Phys. Rev. Lett. **121**, 216001 (2018).
[56] W. H. Press, S. A. Teukolsky, W. T. Vetterling, and B. P. Flannery, *Numerical Recipes in Fortran 90 : The Art of Parallel Scientific Computing*, 2nd ed. (Cambridge University Press, New York, 1996).
[57] L. C. Gallington and A. Bongiorno, J. Chem. Phys. **132**, 174707 (2010).
[58] A. D. Corso, https://github.com/dalcorso/pslibrary.
[59] J. P. Perdew and A. Zunger, Phys. Rev. B **23**, 5048 (1981).
[60] J. P. Perdew, K. Burke, and M. Ernzerhof, Phys. Rev. Lett. **77**, 3865 (1996).
[61] J. P. Perdew, A. Ruzsinszky, G. I. Csonka, O. A. Vydrov, G. E. Scuseria, L. A. Constantin, X. Zhou, and K. Burke, Phys. Rev. Lett. **100**, 136406 (2008).
[62] S. Baroni, S. de Gironcoli, A. Dal Corso, and P. Giannozzi, Rev. Mod. Phys. **73**, 515 (2001).
[63] Y. Okada and Y. Tokumaru, J. Appl. Phys. **56**, 314 (1984).
[64] J. J. Hall, Phys. Rev. **161**, 756 (1967).
[65] P. Loubeyre, R. Le Toullec, M. Hanfland, L. Ulivi, F. Datchi, and D. Hausermann, Phys. Rev. B **57**, 10403 (1998).
[66] B. W. James and H. Kheyrandish, J. Phys. C: Solid State Phys. **15**, 6321 (1982).
[67] A. Bosak, M. Krisch, M. Mohr, J. Maultzsch, and C. Thomsen, Phys. Rev. B **75**, 153408 (2007).
[68] B. Monserrat, N. D. Drummond, and R. J. Needs, Phys. Rev. B **87**, 144302 (2013).
[69] H. Dammak, E. Antoshchenkova, M. Hayoun, and F. Finocchi, J. Phys.: Condens. Matter **24**, 435402 (2012).

[70] G. Savini, Y. J. Dappe, S. Öberg, J.-C. Charlier, M. I. Katsnelson, and A. Fasolino, Carbon **49**, 62 (2011).
[71] C. S. G. Cousins and M. I. Heggie, Phys. Rev. B **67**, 024109 (2003).
[72] A. I. Korobov, V. M. Prokhorov, A. I. Kokshaiskiy, and N. V. Shirgina, Mater. Today: Proc. **5**, 25966 (2018).
[73] D. S. Kim, O. Hellman, J. Herriman, H. L. Smith, J. Y. Y. Lin, N. Shulumba, J. L. Niedziela, C. W. Li, D. L. Abernathy, and B. Fultz, Proc. Natl. Acad. Sci. U.S.A. **115**, 1992 (2018).
[74] T. Middelmann, A. Walkov, G. Bartl, and R. Schödel, Phys. Rev. B **92**, 174113 (2015).
[75] H. Watanabe, N. Yamada, and M. Okaji, Int. J. Thermophys. **25**, 221 (2004).
[76] D. K. Smith and H. R. Leider, J. Appl. Crystallogr. **1**, 246 (1968).
[77] A. C. Bailey and B. Yates, J. Appl. Phys. **41**, 5088 (1970).
[78] G. Shukla, Z. Wu, H. Hsu, A. Floris, M. Cococcioni, and R. M. Wentzcovitch, Geophys. Res. Lett. **42**, 1741 (2015).
[79] A. R. Oganov, J. P. Brodholt, and G. D. Price, Nature (London) **411**, 934 (2001).
[80] X. Li, S. Schönecker, W. Li, L. K. Varga, D. L. Irving, and L. Vitos, Phys. Rev. B **97**, 094102 (2018).